JCTC Journal of Chemical Theory and Computation

Article

pubs.acs.org/JCTC

Photodissociation Dynamics of Homonuclear Diatomic Molecules in Helium Nanodroplets. The Case of $Cl_2@(^4He)_N$

Arnau Vilà,[†] Miguel González,*[,†] and Ricardo Mayol*[,‡]

[†]Departament de Química Física i IQTC and [‡]Departament d'Estructura i Constituents de la Matèria, Universitat de Barcelona, c/Martí i Franquès, 1, 08028 Barcelona, Spain

Supporting Information

ABSTRACT: To investigate the photodissociation dynamics of diatomic homonuclear molecules in helium nanodroplets, a hybrid quantum mechanical theoretical method that combines time dependent density functional theory (helium) and quantum dynamics (molecule) has been developed. This method has been applied to investigate the Cl_2 photodissociation arising from the B ← X electronic transition, considering $Cl_2(v = 0,X)@(^4He)_N$ nanodroplets with N = 50, 100, 200, 300, and 500 (initial configuration for the dynamics). A time scale of a few picoseconds has been determined, and the time required for the dissociating atoms to reach the nanodroplet surface increases with N. Moreover, at the high velocities involved (orders of magnitude above the Landau's critical velocity), an efficient energy exchange between the chlorine atoms and the helium takes place, releasing up to 91% of the energy of the excited diatomics for the bigger nanodroplet considered; and the energy exchange mechanism is the same for all the nanodroplets. Finally, simple (linear) relations for the average Cl final velocity and the (small) number of evaporated He atoms with respect to the radius of the droplets have been reported, together with the existence of confinement resonances. We hope that these results will encourage the experimentalists to investigate this kind of systems.

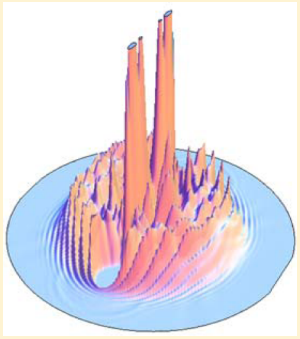

1. INTRODUCTION

The study of helium nanodroplets has become an active area of research since the first experiments, which were performed in the early 1990s of the last century.[1−3] Apart from its fundamental interest, being a quantum liquid system of intermediate size (between bulk liquid and molecular clusters), these droplets have attracted the interest of many investigators for the applications they provide acting as a matrix, due to its facility to pick up almost any chemical specie. The inert chemical character of helium together with the superfluidity[4] of these nanoscopic systems make them very useful to carry out high resolution spectroscopy studies[5] of chemical species embedded in these nanodroplets. A lot of work has been done in this context, both from the experimental and theoretical perspectives, providing information not only about the embedded species but also about the solvation structure and other properties of these nanoscopic systems.

On the other hand, a wide variety of chemical processes has been investigated experimentally.[6−8] Moreover, from the perspective of the chemical synthesis, the encounter of reactants is facilitated by the ability of helium droplets to be doped with the majority of chemical species and by the tendency of most dopants to be placed in the center of the droplet. The evaporation of some ^4He atoms allows the excess of energy to be dissipated, stabilizing complexes that would not be stable in gas phase. In this context many efforts have been made to investigate, e.g., reactions of inorganic clusters,[9] synthesis of metallic nanoclusters,[10] nanowires,[11] entrance channel van der Waals complexes (X-HF, X = Cl, Br, I)[12] and polymers.[13] Nevertheless, these studies were focused on the synthesis of novel chemical species, rather than on the investigation of the reaction dynamics in the quantum fluid. To date, little effort has been devoted to this topic.[14] Thus, to the best of our knowledge, only a set of experimental reaction dynamics studies has been reported so far (photodissociation of alkyl iodides in helium nanodroplets).[8,15,16] From a theoretical point of view, only a single study has been reported in the literature on this field,[17] considering the same system investigated here, but using a very different methodology and taking into account strongly different physical conditions (nonsuperfluid helium nanodroplets (T = 4 K) containing up to 200 ^4He atoms), where significant quantum effects were found.

Here, we present a theoretical study of a prototypic and relatively simple reaction, corresponding to the adiabatic photodissociation of a homonuclear diatomic molecule embedded in superfluid helium nanodroplets (T = 0.37 K), i.e., $X_2(\text{ground state})@(^4He)_N + h\nu \rightarrow X_2(\text{excited state})@(^4He)_N \rightarrow 2X + (^4He)_{N'} + (N-N')\ ^4He$, where the last term simply refers to the total number of vaporized He atoms (maximum N value of 500). In order to do this we have coupled one of the main methods used to describe relatively large systems of bosonic liquid helium and a usual procedure in gas phase quantum reaction dynamics. More concretely, a hybrid approach using the density functional theory (DFT) for

Received: December 21, 2014

DOI: 10.1021/ct5011642
J. Chem. Theory Comput. XXXX, XXX, XXX−XXX

the description of the superfluid ^{4}He system[18] and a quantum wave packet dynamics[19] for the description of the X_2 molecule has been proposed. The DFT method allows us to deal with nanodroplets of big sizes, from a hundred to thousands of helium atoms, depending on the system and the process considered, obtaining a good compromise between accuracy and computational cost. These nanodroplet sizes are in a rather good correspondence with the ones employed in the experiments and so the simulations take into account the fully solvated nature of the X_2 dopant during the photodissociation process. As a particular example, we have studied the interesting case of the $Cl_2(X^1\Sigma_g^+) + h\nu \rightarrow Cl_2(B^3\Pi_u(0)_u^+)) \rightarrow Cl(^2P_{3/2}) + Cl(^2P_{1/2})$ photodissociation process ($\lambda \approx 400$ nm (3.10 eV)) in helium nanodroplets of different sizes (cf. potential energy curves of Cl_2[20] in Figure 1).

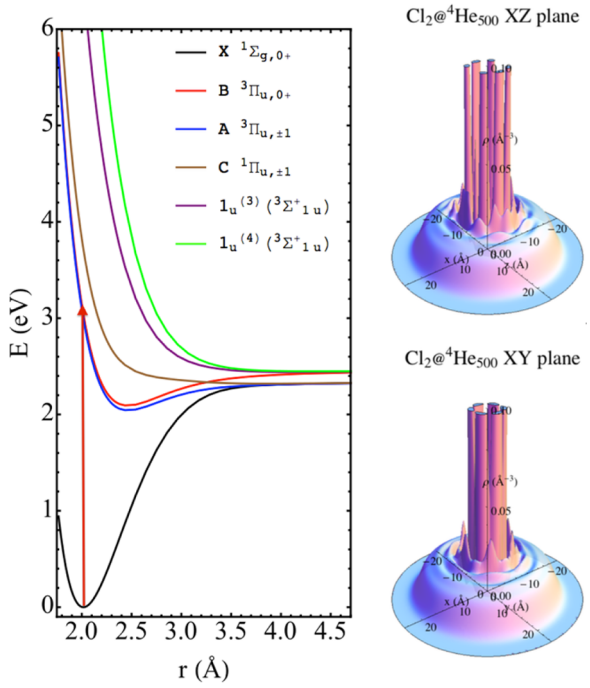

Figure 1. Left panel: ground (X) and five lowest excited (A, B, C, $1_u^{(3)}$, and $1_u^{(4)}$) potential energy curves of Cl_2, including relativistic corrections, where the arrow shows the B ← X electronic transition (data taken from ref 20). The vibrational energy of the initial state of $Cl_2(X, v = 0)$ is 0.035 eV. The two Cl_2 dissociation limits shown correspond to $Cl(^2P_{3/2}) + Cl(^2P_{3/2})$ (ground state atoms) and $Cl(^2P_{3/2}) + Cl(^2P_{1/2})$ (ground and excited atoms, respectively). Right panel: helium density for $Cl_2(X, v = 0)@(^4He)_{500}$ in the *xz* and *xy* planes (the molecule is found in the center of the nanodroplet and along the *z* axis).

The type of process considered here is a good starting point for the theoretical investigation of the reaction dynamics in helium nanodroplets as, in addition of its interest, it is less complex than a bimolecular process. Besides, from the experimental point of view, we expect this process to be not so much complicated to be studied and have well controlled reaction conditions and chemical and physical properties measurements. In contrast to this, in the case of bimolecular reactions, which involve two pick-up steps, the conditions would not be so well-defined. On the other hand, the symmetry of the $X_2@^4He_N$ systems reduces the computational cost. Thus, it will be seen that only the X-X relative coordinate wave packet is needed to describe the evolution of the diatomic molecule along the dissociation axis (cf. Section 2).

2. THEORETICAL METHODS

There are several steps implied in the experimental study of the photodissociation of a homonuclear diatomic molecule X_2 embedded in helium nanodroplets. The first one consists in the production of nanodroplets by supersonic expansion of He gas through a nozzle. Once the nanodroplets are generated, the next step is the picking up of the molecule and the following relaxation mediated by evaporation of some helium atoms. After that, for a given doped nanodroplet, $X_2@(^4He)_N$, a suitable laser photon ($h\nu$) induces the electronic transition of X_2 from the ground electronic state to a selected excited state, which leads to the dissociation of the two X atoms and the evaporation of several He atoms, i.e., $2X + (^4He)_{N'} + (N-N')\ ^4He$. Finally, the resulting helium nanodroplet, $(^4He)_{N'}$, suffers a relaxation process in which it loses the excess of energy by evaporation of some additional helium atoms.

In the present work, we have focused on the dynamics of the photodissociation step employing a full quantum mechanical treatment. The helium description is based on the DFT, using the so-called Orsay-Trento functional[18] ($T = 0$ K) to account for the properties of the helium superfluid, with a modification that allows to describe the formation of solid-like structures (snowballs), when the interaction between the impurity and the helium is strong.[21] The backflow and kinetic correlation terms of this functional have been neglected for computational reasons, as usual.[22,23] The consequence of not including the backflow term is the increasing of the Landau's critical velocity for the bulk liquid ^{4}He.[22] The description of the diatomic molecule is based on the relative coordinate (Cl−Cl distance in this case) wave function, owing to the symmetry of the system. In the first study of this type of processes in superfluid helium nanodroplets we do not have considered the X_2 rotational degree of freedom (of course, the very low temperature of the nanodroplets (around 0.37 K) makes the $j = 0$ rotational state to be, essentially, the only populated one in the diatomic electronic ground state). Moreover, the rotational motion of the Cl_2 free molecule is very slow compared to the time scale of photodissociation. Thus, the rotational period of Cl_2 ($j = 1$) is about 68 and 103 ps for the X and B states, respectively ($\tau_{rot} \approx h/2B_e$, where B_e is the rotational constant).

The potential energy surfaces (PESs) describing the interaction potential between the helium atom and the selected molecule in the ground and excited electronic states (He−Cl_2(X) and He−Cl_2(B) PESs, respectively) have been taken from ref 24. The structure and energetics of the nanodroplets, in general, depend in an important way on the electronic state of the atomic or molecular embedded species (see, e.g., ref 25).

As a starting point for the reaction dynamics study, we have determined the structure and energy of the system in the ground state, $Cl_2(X)@(^4He)_N$. We have treated the molecule as an external potential[25] (with internal structure (vibration)) for the helium nanodroplet, and the center of mass (CM) degree of freedom of the molecule has been treated classically, because of its large effective mass ($2m_{Cl}$) compared to the helium atom mass. Concerning the relative coordinate, it has been described by its corresponding wave function $\varphi_{Cl_2}(r)$, and the vibrationally adiabatic approximation (see, e.g., ref 26) has been used. This simplification is sound since the energy perturbation made by the helium solvation on the diatomic molecule is much smaller

DOI: 10.1021/ct5011642
J. Chem. Theory Comput. XXXX, XXX, XXX−XXX

than the diatomic potential energy, which results in the decoupling of the vibrational degree of freedom. So that, we selected the $v = 0$ vibrational wave function of the free (gas phase) molecule to describe the embedded molecule.

Therefore, to determine the ground state of the system (static part of the calculation) we have to optimize the ^{4}He density, taking into account the interaction potential arising from the $Cl_2(X^1\Sigma_g^+, v = 0, j = 0)$ molecule. The pseudo-Schrödinger equation to be solved that provides this ground state is found by performing a minimization of the energy functional (eq 3), varying the helium density while keeping the number of helium atoms in the droplet constant.

This yields the following expression

$$\left[-\frac{\hbar^2}{2m_{He}}\nabla^2 + \int \mathrm{d}r V_{He-Cl_2(X)}(r, \boldsymbol{R}_{He})|\varphi_{Cl_2(X,v=0)}(r)|^2 + \frac{\delta\varepsilon_c[\rho_{He}]}{\delta\rho_{He}}\right]\sqrt{\rho(\boldsymbol{R}_{He})} = \mu_{He}\sqrt{\rho(\boldsymbol{R}_{He})} \tag{1}$$

where μ_{He} stands for the chemical potential of helium, and $(\delta\varepsilon_c[\rho_{He}])/(\delta\rho_{He})$ is the functional derivative of the helium energy functional. This equation has been solved by means of the imaginary time step propagation method. From these calculations it was obtained that the Cl_2 molecule in the electronic ground state is always found in the center of the nanodroplet, independently of the nanodroplet size. This will simplify the subsequent photodissociation dynamics study because, due to the symmetry of the problem, the CM of the molecule will remain unchanged.

The dynamical process begins with the B ← X electronic transition of Cl_2. We have assumed the Franck−Condon principle (sudden vertical electronic excitation process) and because of this both the Cl_2 vibrational wave function and helium density are kept frozen during the electronic transition. This leads to the $[Cl_2(B)@(^4He)_N]^*$ nanodroplet which has a significant excess of energy with respect to that in the equilibrium configuration $(Cl_2(B)@(^4He)_N)$. Once the B ← X excitation occurs, the $Cl_2(B)$ energy is 11094 K (199 K correspond to kinetic energy), and the $Cl_2(B)$-$(^4He)_N$ interaction energy is, e.g., equal to −388.7 K ($N = 100$) and −421.5 K ($N = 500$). Furthermore, electronic adiabaticity is also considered for $Cl_2(B)$ based on the weak coupling of the B state with the other electronic states of the molecule. The framework used to describe this real time evolution is based on the time dependent DFT (TDDFT) approach, as we have already mentioned. To obtain the governing equations of motion the least action principle is used. The quantum action of the system depends on two functions and is defined as

$$\mathcal{A}[\Psi_{He}, \varphi_{Cl_2}] = \int \mathrm{d}t\left\{E[\Psi_{He}, \varphi_{Cl_2}] - i\hbar\int \mathrm{d}\boldsymbol{R}_{He}\Psi^*_{He}(\boldsymbol{R}_{He})\frac{\partial}{\partial t}\Psi_{He}(\boldsymbol{R}_{He}) - i\hbar\int \mathrm{d}r\varphi^*_{Cl_2}(r)\frac{\partial}{\partial t}\varphi_{Cl_2}(r)\right\} \tag{2}$$

with

$$E[\Psi_{He}, \varphi_{Cl_2}] = \frac{\hbar^2}{2m_{He}}\int \mathrm{d}\boldsymbol{R}_{He}|\nabla\Psi_{He}|^2 + \int \mathrm{d}\boldsymbol{R}_{He}\varepsilon_c[\rho_{He}] + \int \mathrm{d}\boldsymbol{R}_{He}\int \mathrm{d}r V_{He-Cl_2(B)}(r, \boldsymbol{R}_{He})\rho_{He}(\boldsymbol{R}_{He})|\varphi_{Cl_2}(r)|^2 - \frac{\hbar^2}{m_{Cl_2}}\int \mathrm{d}r\varphi^*_{Cl_2}(r)\frac{\partial^2}{\partial r^2}\varphi_{Cl_2}(r) + \int \mathrm{d}r V_{Cl_2(B)}(r)|\varphi_{Cl_2}(r)|^2 \tag{3}$$

where $\rho_{He}(\boldsymbol{R}_{He})$ and $\varepsilon_c[\rho_{He}]$ are the density and the sum of the correlation and potential energy densities of liquid ^{4}He, respectively. This last term accounts for the potential and the strong correlation energies between the helium atoms in the superfluid state. Here, the functional dependence is defined in terms of the ^{4}He effective complex wave function $\Psi_{He}(\boldsymbol{R}_{He}, t) \equiv (\rho_{He}(\boldsymbol{R}_{He}, t))^{1/2}$ and the diatomic wave packet $\varphi_{Cl_2}(r,t)$. Considering variations with respect to these two functions, two coupled Schrödinger-like time dependent dynamical equations are obtained for the helium and chlorine molecule, respectively:

$$i\hbar\frac{\partial}{\partial t}\Psi_{He}(\boldsymbol{R}_{He}) = \left[-\frac{\hbar^2}{2m_{He}}\nabla^2 + \int \mathrm{d}r V_{He-Cl_2(B)}(r, \boldsymbol{R}_{He})|\varphi_{Cl_2}(r)|^2 + \frac{\delta\mathcal{E}_c[\rho_{He}]}{\delta\rho_{He}}\right]\Psi_{He}(\boldsymbol{R}_{He}) \tag{4a}$$

$$i\hbar\frac{\partial}{\partial t}\varphi_{Cl_2}(r) = \left[-\frac{\hbar^2}{m_{Cl_2}}\frac{\partial^2}{\partial r^2} + \int \mathrm{d}\boldsymbol{R}_{He}V_{He-Cl_2(B)}(r, \boldsymbol{R}_{He})\rho_{He}(\boldsymbol{R}_{He}) + V_{Cl_2(B)}(r)\right]\varphi_{Cl_2}(r) \tag{4b}$$

These equations have been solved numerically by discretization of the space in a grid of points for each degree of freedom. The diatomic molecule has been placed along the z axis, and the grid for the relative coordinate is spaced by 0.0174 Å. For the helium part we have worked with Cartesian coordinates, using a spatial separation of 0.35 Å for the x and y axis and 0.09 Å for the z axis. The numerical integrator used is a fourth order Adams predictor-corrector method,[27] initiated by a Runge−Kutta method of fourth order[28] (time step = 1.5×10^{-5} ps). The evaluation of the derivatives for the kinetic energy terms has been carried out in momentum space, performing a Fourier transform using the FFTW package of ref 29. This strategy is useful not only from the point of view of the computational cost but also because it allows to check the quality of the derivatives.

To finish with the computational details, it is worth noting that quartic negative imaginary potentials (NIPs) have been employed in order to avoid artificial reflections of the molecular and helium wave functions at the grid edges[30]

$$V_{NIP} = -iA\frac{5}{2}\left(\frac{d - d_{NIP}}{L}\right)^4 \tag{5}$$

for $d > d_{NIP}$, where the absorption strength (A) is equal to 5171.4 and 3315.0 K Å^{-4} for the molecule and helium, respectively, and the length (L) and location (d_{NIP}) of the NIPs are indicated below. The molecular NIP has been placed in the z axis at a distance of 12.0 Å with respect to the nanodroplet surface and has a length of 1.1 Å. The NIPs for helium have been located in the z axis at a distance of 12.0 Å with respect to

DOI: 10.1021/ct5011642
J. Chem. Theory Comput. XXXX, XXX, XXX−XXX

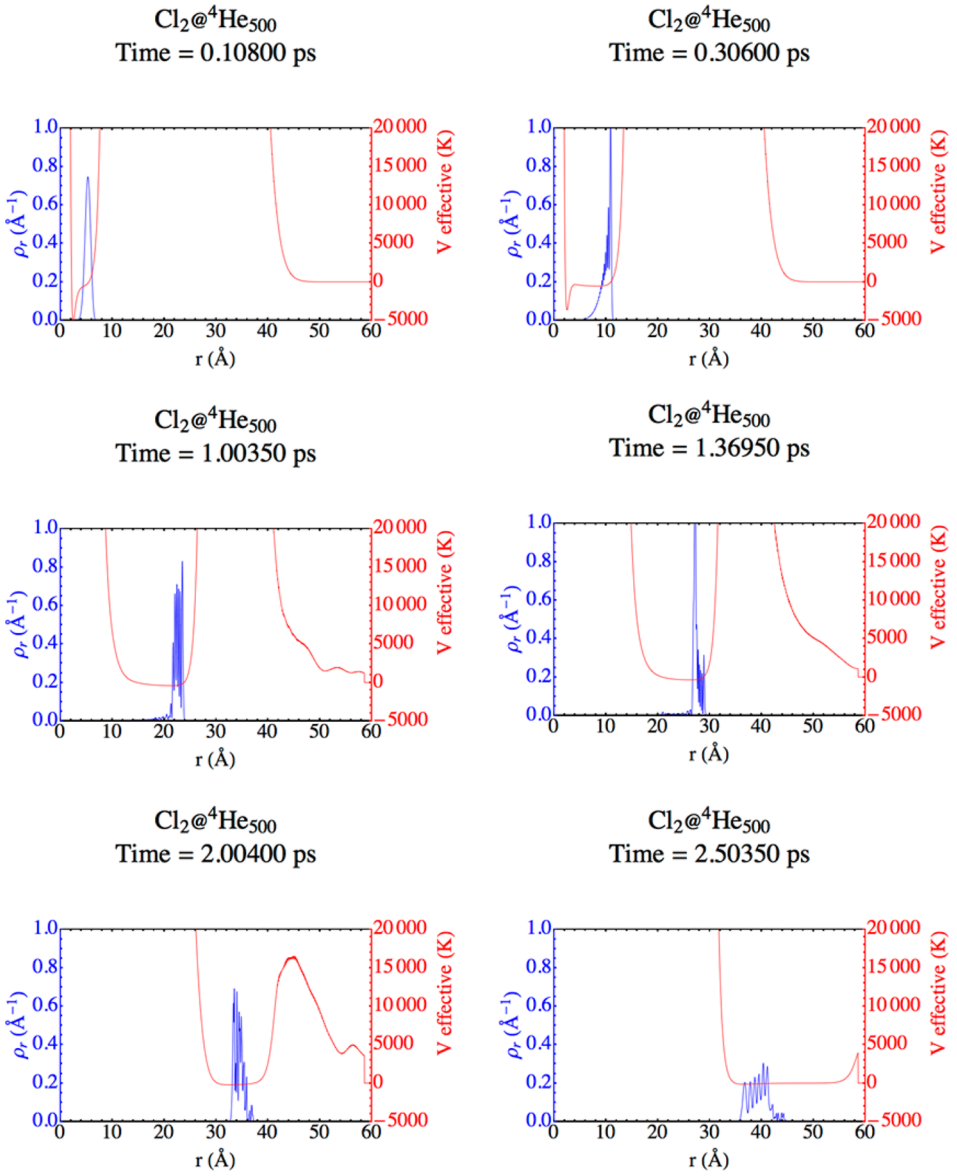

Figure 2. Snapshots showing the time evolution of the squared modulus of the relative coordinate wave packet (blue) and effective potential (red), during nearly all the $[Cl_2(B)@(^4He)_{500}]^*$ photodissociation process. See also movie 1 (SI).

the surface (length of 3.3 Å), while in the x and y axis they have been placed at 6.0 Å (length of 3.3 Å).

The final photofragment (Cl) velocity distribution has been obtained from the Cl_2 wave function, expressed in momentum representation, before applying the molecular NIP. Moreover, a flux analysis has been performed to check the quality of the propagation, using the continuity equation $((\partial/\partial t)\rho_{Cl_2} + (\partial/\partial r)\, j_{Cl_2} = 0)$.

3. RESULTS AND DISCUSSION

We have studied theoretically the photodissociation dynamics of Cl_2 in helium nanodroplets of different sizes: $Cl_2(X)@(^4He)_N + h\nu \rightarrow [Cl_2(B)@(^4He)_N]^* \rightarrow Cl(^2P_{3/2}) + Cl(^2P_{1/2}) + (^4He)_{N'} + (N-N')\ ^4He$, with N = 50, 100, 200, 300, and 500. Although the smaller experimental nanodroplets are formed with around 500 helium atoms, the analysis of the results achieved for the selected systems can show the main features and patterns of the properties related to the nanodroplet size.

The microscopic mechanism of the investigated process can be elucidated quite well from Figures 2 and 3 and the two movies included in the SI, which correspond to the $[Cl_2(B)@(^4He)_{500}]^*$ case, although the general trends described here also apply to the other nanodroplets, unless otherwise indicated. The time evolution of the Cl_2 wave packet (relative coordinate, r, probability density) takes place along the z axis and is shown in Figure 2 together with the effective potential that governs the dynamics of this degree of freedom, i.e., the sum of the Cl_2 potential energy (B state) and the Cl_2-helium interaction potential (which depends on time due to the evolution of the nanodroplet density).

Strong oscillations are produced in the wave packet due to the collision with the first solvation shell (cf. Figure 2 and movie 1 (t = 0.24 ps)), and its shape changes when it becomes close to the nanodroplet surface. Thus, with the exception of what happens for the smaller droplets (N = 50 and 100), the most intense peak changes from the "head" (higher r) to the "tail" (smaller r) region of the wave packet (cf. Figure 2 and

DOI: 10.1021/ct5011642
J. Chem. Theory Comput. XXXX, XXX, XXX−XXX

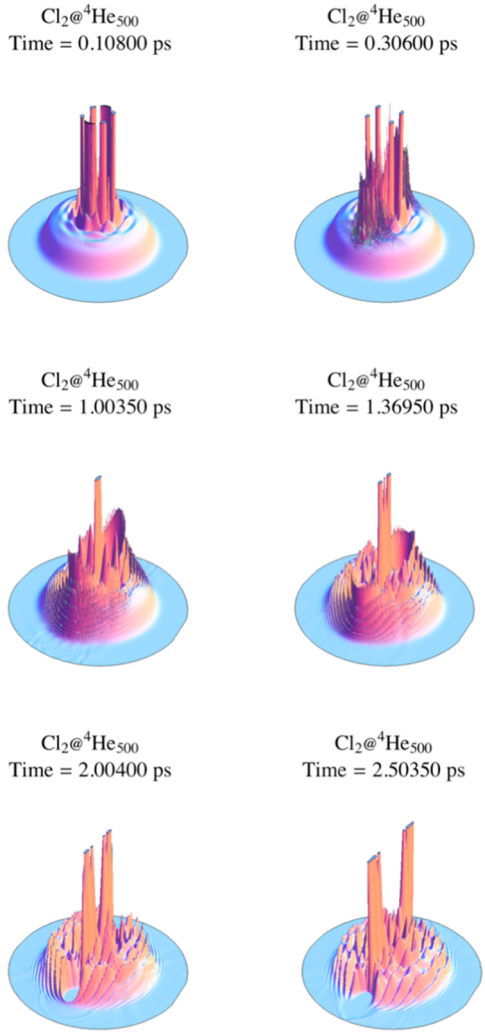

Figure 3. Snapshots showing the time evolution of the helium density (*xz* plane), during nearly all the $[Cl_2(B)@(^4He)_{500}]^*$ photodissociation process. See also movie 2 (SI).

movie 1 (t = 0.94 and 1.20 ps, respectively)). This phenomenon is due to the opening of the cavity (which has been generated inside the nanodroplet by the Cl dissociating atoms) to the exterior of the nanodroplet and the non-equilibrated force balance experienced by each Cl atom when they reach the surface, due to the anisotropy of the surrounding helium density. Another important feature is the confinement provided by the helium environment, which avoids the spatial spreading of the wave packet with time, and differing from what occurs in gas phase translational dynamics.

The time evolution of the helium density (*xz* plane) is represented in Figure 3 and in movie 2 (SI). At the beginning of the process strong distortions are produced in the density, mainly in the vicinity of the z axis. Supersonic shock waves are formed as a consequence of the collision of the wave packet with the first solvation shell. These waves travel at very high velocities (around 4500 m/s), and, when they collide with the nanodroplet surface, some helium density escapes (evaporation process). It can also be observed how the complicated interference pattern motivates the generation of waves traveling in perpendicular direction to the molecular dissociation axis (z axis) and the destruction of the snowball structures. This is facilitated by the freed space between the two Cl atoms, when they separate from each other, that becomes available for helium.

Our results point out that, as a result of the energy transfer between the $Cl_2(B)$ molecule and the helium droplet, a direct escape process is taking place. From the beginning to the end of the photodisociation, it involves the evaporation of some atoms (3 to 10 He atoms from N = 50 to 500, respectively; see below) with a rich energy content, rather than the evaporation of the whole nanodroplet. This is consistent with what has been found in the experiments of ref 8 on the photodissociation of alkyl iodides (R-I → R + I, R = CH_3, CF_3, and C_2H_5; λ = 266 nm (4.66 eV)) in helium nanodroplets.

In Figure 4 the evolution of the expectation value of the Cl−Cl relative velocity with time is represented together with the

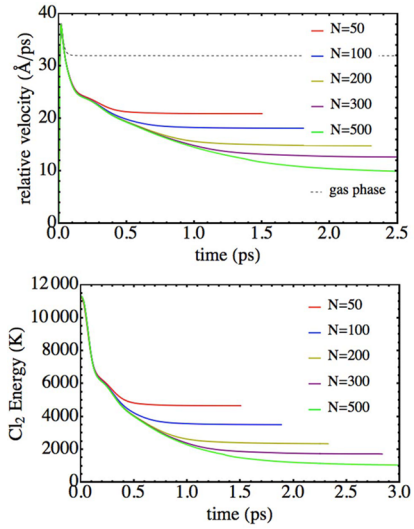

Figure 4. Time evolution of the expectation value of the relative velocity (up) and Cl_2 energy (down) with time for different $[Cl_2(B)@(^4He)_N]^*$ nanodroplet sizes. The gas phase result is also included in the former case (dashed black line).

evolution of the expectation value of the $Cl_2(B)$ energy (kinetic and Cl−Cl interaction energy). The photodissociation process takes place on the picosecond time scale. Thus, in order to reach a Cl−Cl separation of 20 Å, which is one order of magnitude above the initial Cl_2 distance, the $[Cl_2(B)@(^4He)_N]^*$ systems require a similar amount of time (0.8−0.9 ps); while the time required for the Cl dissociating atoms to reach the nanodroplet surface increases with the size (0.85, 1.14, 1.63, 2.01, and 2.57 ps for N = 50, 100, 200, 300, and 500, respectively). This last time has been arbitrarily defined as that one needed by the expectation value of the Cl−Cl distance to be equal to the initial length of the droplet along the z axis, which is taken as twice the corresponding radius (R = 11.0, 13.0, 15.7, 17.5, and 20.04 Å, respectively).

The initial acceleration and deceleration found are governed by the $Cl_2(B)$ potential energy curve, and it is very similar to what happens in the photodissociation evolution in gas phase (cf. Figure 4). This fact points out that, at the beginning (below ≈ 0.035 ps), the process of bond breaking is not appreciably influenced by solvation, due to the high energy difference between the chemical and van der Waals interactions. At somewhat larger times, however, the relative velocity in gas phase becomes constant while that in the droplet decays, indicating that the molecule is exchanging energy with the

DOI: 10.1021/ct5011642
J. Chem. Theory Comput. XXXX, XXX, XXX−XXX

helium. This happens because the velocities involved (1000−3500 m/s) are clearly above (orders of magnitude) the Landau's critical velocity for superfluid (bulk) helium (≈58 m/s (0.58 Å/ps))[31,32] which, on the other hand, has also been observed in helium nanodroplets ($N \approx 1000$ and above).[33]

Comparison of the profiles of the relative velocity (or Cl_2 energy) curves for the different nanodroplet sizes investigated (cf. Figure 4) suggests that the mechanism of energy exchange is the same for all them, as they are very similar to each other. Under these circumstances the helium behavior is similar to that of a conventional liquid (i.e., the fluid viscosity is different from zero) and here this will be more evident when analyzing the expectation value of the Cl−Cl relative velocity vs the expectation value of the Cl−Cl distance. Furthermore, in Figure 4 is also seen that the energy of the dopant is monotonically decreasing, avoiding the possibility of a mechanism in which the solvent and the molecule are exchanging energy back and forth. Finally, we can infer that the fastest energy exchange takes place during the collision with the first solvation shell, which is when the first supersonic waves are produced.

The Cl atomic photofragment velocity distributions are shown in Figure 5. The oscillating shape and presence of an

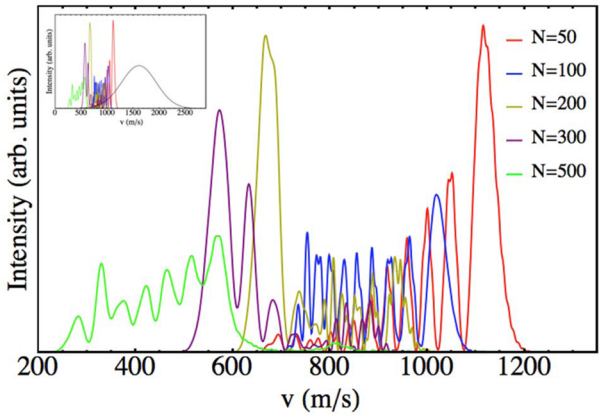

Figure 5. Velocity distributions of the Cl photofragment for different $[Cl_2(B)@(^4He)_N]^*$ nanodroplet sizes. The gas phase result (black line) is also given in the small figure.

important number of peaks in the distributions can be interpreted from the time evolution of the squared modulus of the relative coordinate wave packet expressed in the momentum representation. Thus, a little after (≈0.1 ps) the B ← X electronic transition, a clear oscillating pattern with a significant number of peaks is produced, and, although the contributions of the different momentum values change with time, this behavior is maintained until the final of the photodissociation process, being reflected in the final velocity distribution. These oscillating structures are present for all the nanodroplets, and they probably result from quantum resonances (confinement resonances) arising from the interaction of the $Cl_2(B)$ wave packet with the helium solvent. Although resonances are one of the most striking phenomena in physics and chemistry and resonance analysis is a very interesting topic in reaction dynamics, it is out of the scope of the present work. In fact, this is a very specific and complex analysis,[19,34] even for systems of a small number of degrees of freedom,[35] which is interesting by itself, that will be the subject of a future investigation.

The mean (expectation) values of the Cl velocity distributions are collected in Figure 6a. A quantitative agreement is found when these data are fitted to a $N^{1/3}$ dependence (cf. Figure 7a), suggesting that the mean velocity of the fragments decreases in a proportional manner with the path length of the nanodroplet. With the help of Figure S1 we have verified that his behavior occurs in all cases (and Figure S2 shows the time evolution of the Cl−Cl distance mean value). Thus, we can see that the mean value of the Cl−Cl relative velocity, $\langle v_r \rangle$, depends almost linearly on the mean value of Cl−Cl relative distance, $\langle r \rangle$, for the two $\langle r \rangle$ zones which are defined by the ∼2.6−5.1 Å and ∼6.4−24.5 Å intervals (the higher limit for the second zone is defined by the $N = 500$ case). The same relation, of course, also applies for the mean value of the Cl velocity ($\langle v_{Cl} \rangle = \langle v_r \rangle/2$) vs the mean value of the Cl z-axis coordinate ($\langle z_{Cl} \rangle = \langle r \rangle/2$; Cl atom moving along the positive z-semiaxis).

For each zone, we can write $\langle v_{Cl} \rangle \approx a_0 - a_1 \langle z_{Cl} \rangle$, where a_0 and a_1 are (positive) constants that depend on the zone. Now, if we derive with respect to time and multiply by the atomic mass of Cl (m_{Cl}) both sides of the previous $\langle v_{Cl} \rangle$ expression, we obtain the quantum mechanics analogue of a well known equation describing the force of friction (z component), F_f, acting on a body which is moving, at a given velocity, inside a conventional fluid

$$\langle F_f \rangle \approx -b \langle v_{Cl} \rangle \tag{6}$$

where $b \equiv m_{Cl} a_1$. Hence, for these mean quantities the behavior of the $(^4He)_N$ nanodroplets, at the (large) energies involved in the $Cl_2(B)$ photodissociation, resembles that of a conventional liquid.

In Figure 6b the percentage of energy released from $Cl_2(B)$ to the helium solvent is shown. The large values obtained (57%, 84%, and 91% of the diatomic energy is released to helium for droplets of 50, 300, and 500 He atoms, respectively) point out that the energy exchange mechanism is very efficient. The number of helium atoms evaporated, $N_{He\ evap}$, as a function of the nanodroplet size is collected in Figure 6c. This number increases with the droplet size in a smooth way ($N_{He\ evap} = 3$, 8, and 10 for $N = 50$, 300, and 500, respectively) and follows a $N^{1/3}$ law in a quantitative way (Figure 7c).

To understand this dependence we have considered the following expression $N_{He\ evap} = k(R - R_{cavity})$, where k and R_{cavity} (cavity radius) are constants. This cavity, which is similar to a sphere, corresponds to the volume placed inside the droplet and centered in the Cl_2 molecule in which no helium atoms are found. The term $R - R_{cavity}$ corresponds to the distance traveled by each Cl atom through the helium nanodroplet. By doing this fitting ($N_{He\ evap}$ vs R) we obtained that R_{cavity} is about 4.8 Å, a value that compares quite well with the initial radius of the cavity along the z axis (≈4.6 Å) and shows the plausibility of our hypothesis. Finally, in Figure 6d the mean energy per evaporated ^4He atom is shown, which exhibits a moderate decrease with N (the value for $N = 500$ is nearly half of that obtained for $N = 50$).

4. SUMMARY AND CONCLUSIONS

We have developed a quantum mechanical approach based on a hybrid theoretical method to describe the photodissociation dynamics of a homonuclear diatomic molecule embedded in ^4He superfluid nanodroplets ($T = 0.37$ K). In this way, the time evolution of helium is described within the TDDFT framework,

DOI: 10.1021/ct5011642
J. Chem. Theory Comput. XXXX, XXX, XXX−XXX

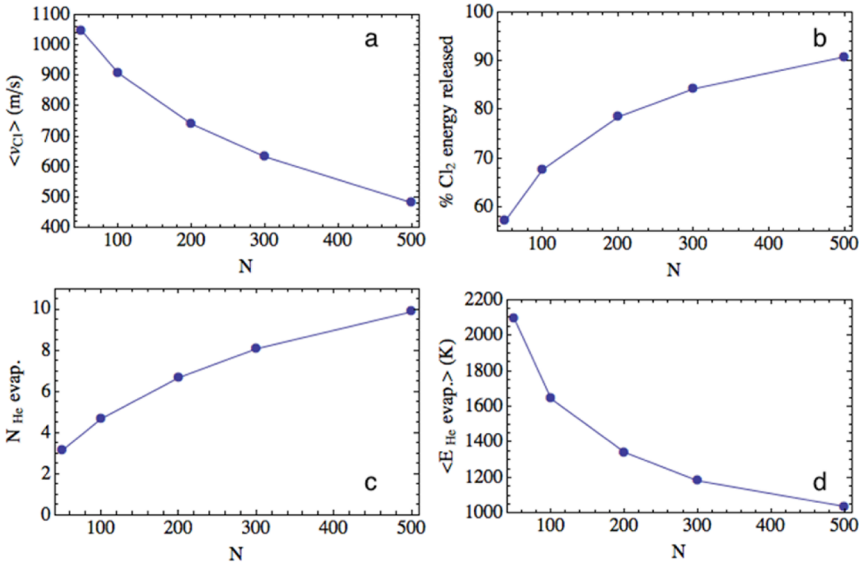

Figure 6. Mean value of the Cl escape velocity (a), percentage of the Cl_2 energy released to the droplet (b), number of ^4He evaporated atoms (c), and mean energy per evaporated ^4He atom (d), for different $[Cl_2(B)@(^4He)_N]^*$ nanodroplet sizes (N = 50, 100, 200, 300, and 500).

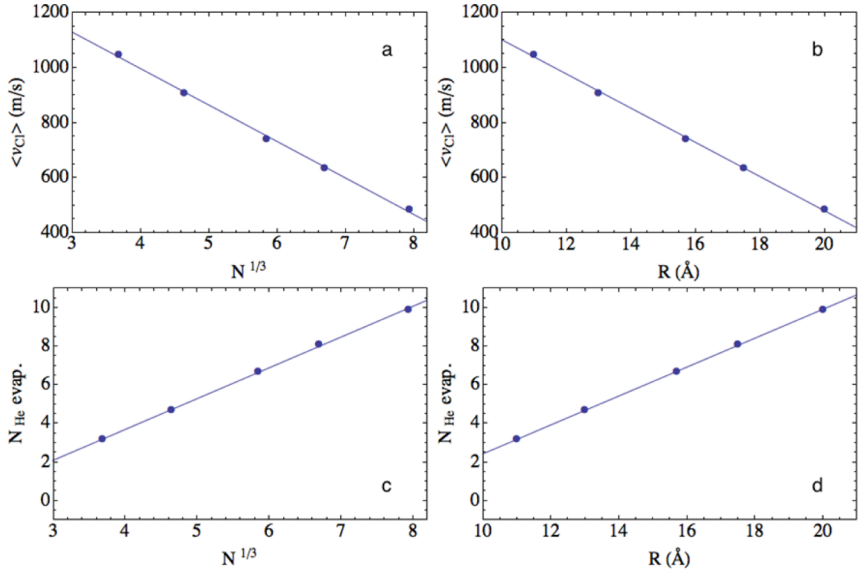

Figure 7. Mean value of the Cl escape velocity as a function of $N^{1/3}$ (a) and R (b), and number of ^4He evaporated atoms as a function of $N^{1/3}$ (c) and R (d), for different $[Cl_2(B)@(^4He)_N]^*$ nanodroplet sizes (N = 50, 100, 200, 300, and 500).

while the time dependent wave packet quantum dynamics is used for the diatomic molecule. Using this hybrid strategy we have studied the interesting case of the Cl_2 photodissociation dynamics, induced by the B ← X electronic transition, for $Cl_2(v = 0,X)@(^4He)_N$ doped nanodroplets, with N ranging from 50 up to 500. These droplets correspond to the initial configuration for the dynamics, and the process takes place on the picosecond time scale. The time required for the Cl dissociating atoms to reach the nanodroplet surface increases with the size (0.85−2.57 ps).

At the large velocities involved, which clearly exceed the Landau's critical velocity, an efficient energy exchange mechanism has been found (e.g., 57% and 91% of the $Cl_2(B)$ energy is released to the helium for N = 50 and 500, respectively), and the energy exchange mechanism is independent of the size of the nanodroplet. Furthermore, simple linear expressions for the average Cl final velocity and the (small) number of evaporated He atoms with respect to the radius of the nanodroplet have been reported, together with the existence of confinement resonances leading to very well-defined sharp structures (strongly oscillating peaks) in the Cl final velocity distribution.

We hope that the present theoretical study will encourage the experimentalists to investigate the reaction dynamics of this and related photodissociation processes.

■ ASSOCIATED CONTENT

Supporting Information

Figures: Expectation value of the Cl−Cl relative velocity as a function of the expectation value of the Cl−Cl distance for different nanodroplet sizes (Figure S1); Time evolution of the Cl−Cl distance expectation value for different nanodroplet sizes (Figure S2). Movies for $[Cl_2(B)@(^4He)_{500}]^*$: Time evolution of the Cl_2 wave packet probability density and effective

DOI: 10.1021/ct5011642
J. Chem. Theory Comput. XXXX, XXX, XXX−XXX

potential (movie 1); Time evolution of the helium density (movie 2). This material is available free of charge via the Internet at http://pubs.acs.org.

AUTHOR INFORMATION

Corresponding Authors

*Fax: 34 93 4021231. E-mail: miguel.gonzalez@ub.edu.
*Fax: 34 93 4037063. E-mail: ricardo.mayol@ub.edu.

Notes

The authors declare no competing financial interest.

ACKNOWLEDGMENTS

This work has been supported by the Spanish Ministry of Science and Innovation (projects refs CTQ2011-27857-C02-01 and FIS2011-28617-C02-01), and we also want to acknowledge the support from the Autonomous Government of Catalonia (A. V. predoctoral fellowship and projects refs 2009SGR 17 and XRQTC). We also thanks Prof. Toshiyuki Takayanagi (Saitama University, Japan) for sharing the code of the potential energy surfaces of the triatomic He−Cl_2(X) and He−Cl_2(B) systems and Prof. Satoshi Yabushita (Keio University, Japan) for sharing the potential energy curves of Cl_2.

REFERENCES

(1) Buchenau, H.; Knuth, E. L.; Northby, J.; Toennies, J. P.; Winkler, C. Mass Spectra and Time-of-Flight Distributions of Helium Cluster Beams. *J. Chem. Phys.* **1990**, *92*, 6875.

(2) Hartmann, M.; Mielke, F.; Toennies, J. P.; Vilesov, F.; Benedek, G. Direct Spectroscopic Observation of Elementary Excitations in Superfluid He Droplets. *Phys. Rev. Lett.* **1996**, *76*, 4560−4563.

(3) Goyal, S.; Schutt, D. L.; Scoles, G. Vibrational Spectroscopy of Sulphur Hexafluoride Attached to Helium Clusters. *Phys. Rev. Lett.* **1992**, *69*, 933−936.

(4) Hartmann, M.; Miller, R. E.; Toennies, J. P.; Vilesov, A. High-Resolution Molecular Spectroscopy of van der Waals Clusters in Liquid Helium Droplets. *Science* **1996**, *272*, 1631−1634.

(5) Toennies, J. P.; Vilesov, A. Superfluid Helium Droplets: A Uniquely Cold Nanomatrix for Molecules and Molecular Complexes. *Angew. Chem., Int. Ed.* **2004**, *43*, 2622−2648.

(6) Krasnokutski, S. A.; Huisken, F. Low-Temperature Chemistry in Helium Droplets: Reactions of Aluminum Atoms with O_2 and H_2O. *J. Phys. Chem. A* **2011**, *115*, 7120−7126.

(7) Lugovoj, E.; Toennies, P. J.; Vilesov, A. Manipulating and Enhancing Chemical Reactions in Helium Droplets. *J. Chem. Phys.* **2000**, *112*, 8217−8220.

(8) Braun, A.; Drabbels, M. Photodissociation of Alkyl Iodides in Helium Nanodroplets. I. Kinetic Energy Transfer. *J. Chem. Phys.* **2007**, *127*, 114303.

(9) Müller, S.; Krapf, S.; Koslowski, Th.; Mudrich, M.; Stienkemeier, F. Cold Reactions of Alkali-Metal and Water Clusters inside Helium Nanodroplets. *Phys. Rev. Lett.* **2009**, *102*, 183401.

(10) Yang, S.; Ellis, A. M.; Spence, D.; Feng, C.; Boatwright, A.; Latimer, E.; Binns, C. Growing Metal Nanoparticles in Superfluid Helium. *Nanoscale* **2013**, *5*, 11545−11553.

(11) Latimer, E.; Spence, D.; Feng, C.; Boatwright, A.; Ellis, A. M.; Yang, S. Preparation of Ultrathin Nanowires Using Superfluid Helium Droplets. *Nano Lett.* **2014**, *14*, 2902−2906.

(12) Merritt, J. M.; Küpper, J.; Miller, R. E. Entrance Channel X-HF (X=Cl, Br and I) Complexes Studied by High-Resolution Infrared Laser Spectroscopy in Helium Nanodroplets. *Phys. Chem. Chem. Phys.* **2005**, *7*, 67−78.

(13) Douberly, G. E.; Miller, R. E. The Growth of HF Polymers in Helium Nanodroplets: Probing the Barriers to Ring Insertion. *J. Phys. Chem. B* **2003**, *107*, 4500−4507.

(14) Yang, S.; Ellis, A. M. Helium Droplets: A Chemical Perspective. *Chem. Soc. Rev.* **2013**, *42*, 472−484.

(15) Braun, A.; Drabbels, M. Photodissociation of Alkyl Iodides in Helium Nanodroplets. II. Solvation Dynamics. *J. Chem. Phys.* **2007**, *127*, 114304.

(16) Braun, A.; Drabbels, M. Photodissociation of Alkyl Iodides in Helium Nanodroplets. III. Recombination. *J. Chem. Phys.* **2007**, *127*, 114305.

(17) Takayanagi, T.; Shiga, M. Photodissociation of Cl_2 in Helium Clusters: An Application of Hybrid Method of Quantum Wavepacket Dynamics and Path Integral Centroid Molecular Dynamics. *Chem. Phys. Lett.* **2003**, *372*, 90−96.

(18) Dalfovo, F.; Lastri, A.; Pricaupenko, L.; Stringari, S.; Treiner, J. Structural and Dynamical Properties of Superfluid Helium: A Density-Functional Approach. *Phys. Rev. B* **1995**, *52*, 1193−1209.

(19) Tannor, D. J. *Introduction to Quantum Mechanics. A Time Dependent Perspective*; University Science Books: Sausalito, CA, 2007.

(20) Asano, Y.; Yabushita, S. Theoretical Study on the Nonadiabatic Transitions in the Photodissociation Processes of Cl_2. *J. Phys. Chem. A* **2001**, *105*, 9873−9882.

(21) Ancilotto, F.; Barranco, M.; Caupin, F.; Mayol, R.; Pi, M. Freezing of ^{4}He and its Liquid-Solid Interface from Density Functional Theory. *Phys. Rev. B* **2005**, *72*, 214522.

(22) Mateo, D.; Hernando, A.; Barranco, M.; Loginov, E.; Drabbels, M.; Pi, M. Translational Dynamics of Photoexcited Atoms in ^{4}He Nanodroplets: The Case of Silver. *Phys. Chem. Chem. Phys.* **2013**, *15*, 18388−18400.

(23) Mateo, D.; Gonzalez, F.; Eloranta, J. Rotational Superfluidity in Small Helium Droplets. *J. Phys. Chem. A* **2014**, DOI: 10.1021/jp5057286.

(24) Williams, J.; Rohrbacher, A.; Seong, J.; Marianayagam, N.; Janda, K. C.; Burcl, R.; Szcześniak, M. M.; Chałasiński, G.; Cybulski, S. M.; Halberstadt, N. A Three-Dimensional Potential Energy Surface for He + Cl_2 ($B^3\Pi_{0u+}$): Ab Initio Calculations and a Multiproperty Fit. *J. Chem. Phys.* **1999**, *111*, 997−1007.

(25) Vilà, A.; González, M.; Mayol, R.; Paniagua, M. Theoretical Approach to the Structure, Energy and Electronic Spectroscopy of O@(^{4}He)$_N$ Doped Nanodroplets. *RSC Adv.* **2014**, *4*, 44972−44979.

(26) Paesani, F.; Gianturco, F. A. Vibrational Effects in a Weakly-Interactiong Quantum Solvent: The CO Molecule in ^{4}He Gas and in ^{4}He Droplets. *J. Chem. Phys.* **2002**, *116*, 10170−10182.

(27) Ralston, A.; Numerical Integration Methods for the Solution of Ordinary Differential Equations. In *Mathematical Methods for Digital Computers*; Ralston, A., Wilf, H. S., Eds.; John Wiley & Sons: New York, 1960; Vol. No. 1, pp 95−109.

(28) Thompson, R. J. Improving Round-off in Runge-Kutta Computations with Gill's Method. *Commun. ACM* **1970**, *13*, 739−740.

(29) Frigo, M.; Johnson, S. G. The Design and Implementation of FFTW3. *IEEE Proceedings* **2005**, *93*, 216−231.

(30) Vibók, A.; Balint-Kurti, G. G. Parametrization of Complex Absorbing Potentials for Time-Dependent Quantum Dynamics. *J. Phys. Chem.* **1992**, *96*, 8712−8719.

(31) Tilley, D. R.; Tilley, J. Condensates and Excitations. *Superfluidity and Superconductivity*; Institut of Physics Publishing: Bristol, U. K., 1990; pp 41−53.

(32) Annet, J. F. Superfluid Helium-4. *Superconductivity, Superfluids and Condensates*; Oxford University Press: Oxford, U. K., 2004; pp 38−43.

(33) Brauer, N. B.; Smolarek, S.; Loginov, E.; Mateo, D.; Hernando, A.; Pi, M.; Barranco, M.; Buma, W. J.; Drabbels, M. Critical Landau Velocity in Helium Nanodroplets. *Phys. Rev. Lett.* **2013**, *111*, 153002.

(34) Moiseyev, N. *Non-Hermitian Quantum Mechanics*; Cambridge University Press: Cambridge, U. K., 2011.

(35) Gamallo, P.; Huarte-Larrañaga, F.; González, M. Resonances in the Ne + H_2^+ → NeH^+ + H Proton-Transfer Reaction. *J. Phys. Chem. A* **2013**, *117*, 5393−5400.

DOI: 10.1021/ct5011642
J. Chem. Theory Comput. XXXX, XXX, XXX−XXX